AGU PUBLICATIONS

Water Resources Research

RESEARCH ARTICLE
10.1002/2013WR014293

Key Points:
- A process-based, coupled surface-subsurface, 2-D mathematical model is presented
- The model effectively integrates the main hydrologic and hydraulic processes
- The model can be applied to storm events in rural lowland catchments

Correspondence to:
D. P. Viero,
daniele.viero@unipd.it

Citation:
Viero, D. P., P. Peruzzo, L. Carniello, and A. Defina (2014), Integrated mathematical modeling of hydrological and hydrodynamic response to rainfall events in rural lowland catchments, *Water Resour. Res.*, *50*, doi:10.1002/2013WR014293.

Received 19 JUN 2013
Accepted 30 JUN 2014
Accepted article online 2 JUL 2014

Integrated mathematical modeling of hydrological and hydrodynamic response to rainfall events in rural lowland catchments

D. P. Viero[1], P. Peruzzo[1], L. Carniello[1], and A. Defina[1]

[1]Department of Civil, Environmental, and Architectural Engineering, University of Padova, Padova, Italy

Abstract In rural lowland catchments, negligible topographic gradients and possible interactions between overland and channel flows complicate efforts to predict flood formation, propagation, and inundation. In this study, we demonstrate that an approach in which a two-dimensional shallow water model is coupled with a two-dimensional model for the saturated flow in the topsoil layer can accurately reproduce floods in such a lowland catchment. The topsoil porous layer is treated as a confined aquifer where water ponds on the ground surface and as an unconfined aquifer elsewhere. The model includes infiltration from the ground surface into the topsoil layer and downward percolation out of the topsoil layer. The equations of both surface and subsurface models are suitably averaged over a representative elementary area to yield a subgrid model for the coupled surface-subsurface flow. Field data collected in two rural lowland catchments in the North-East of Italy are used to evaluate the model performance. The good agreement between computed and measured discharge at the catchments' outlet and the agreement between predicted and surveyed spatial pattern of inundated areas indicate that the model effectively reproduces overland flow and efficiently accounts for the surface-subsurface flow interaction and the relevant subsurface processes.

1. Introduction

Physically based mathematical models for flood inundation of lowland areas are the most effective and commonly used tools to assess hydraulic vulnerability, to design intervention plans, or to support management and operational decisions [see e.g., *Hunter et al.*, 2007, and references therein]. Such models solve the shallow water equations over two-dimensional (2-D) computational domains. Specific algorithms are often included to describe the wetting and drying process and to couple 2-D and one-dimensional (1-D) features. In rural lowland catchments, typically criss-crossed by drainage channels, the focus is usually on the whole channel network. In this case (Figure 1, left), all channels of the network are divided into segments: for each segment the tributary basin has to be identified and the corresponding inflow hydrograph is prescribed as a boundary condition [see e.g., *Lerat et al.*, 2012, and references therein]. The estimation of inflow hydrographs from rainfall data is commonly carried out by using rainfall-runoff models, either distributed or lumped [see e.g., *Bates and De Roo*, 2000; *McMillan and Brasington*, 2008; *Grimaldi et al.*, 2013]. Accordingly, the prediction of inundation uses an uncoupled approach since runoff production (i.e., inflow hydrograph) is not affected by and does not affect the inundation of the tributary basin.

This uncoupled approach suffers from a number of problems, which are especially serious in the case of flooding of rural lowland areas. Indeed, the identification of subcatchments is often uncertain due to negligible topographic gradients: great care and sophisticated tools, along with high-resolution digital elevation models, are necessary to accurately characterize the subcatchments by identifying linear structures (ditches, furrows, etc.), flow directions and pathways, and contributing areas [see e.g., *Duke et al.*, 2006; *Getirana et al.*, 2009; *Gascuel-Odoux et al.*, 2011; *Cazorzi et al.*, 2013; *Schwanghart et al.*, 2013]. Moreover, small topographic gradients also enhance the mutual interaction between runoff production and inundation, which is not considered in the uncoupled approach. The uncoupled approach often assumes that the excess rainfall is delivered from the landscape to the modeled channel network; i.e., it assumes that the smaller, not modeled, drainage system composed of ditches and furrows is fully capable of draining the land. Actually, sophisticated hydrologic models can account for the dynamical interaction between the sequence of states experienced by a catchment and its hydrologic response, including surface ponding induced by

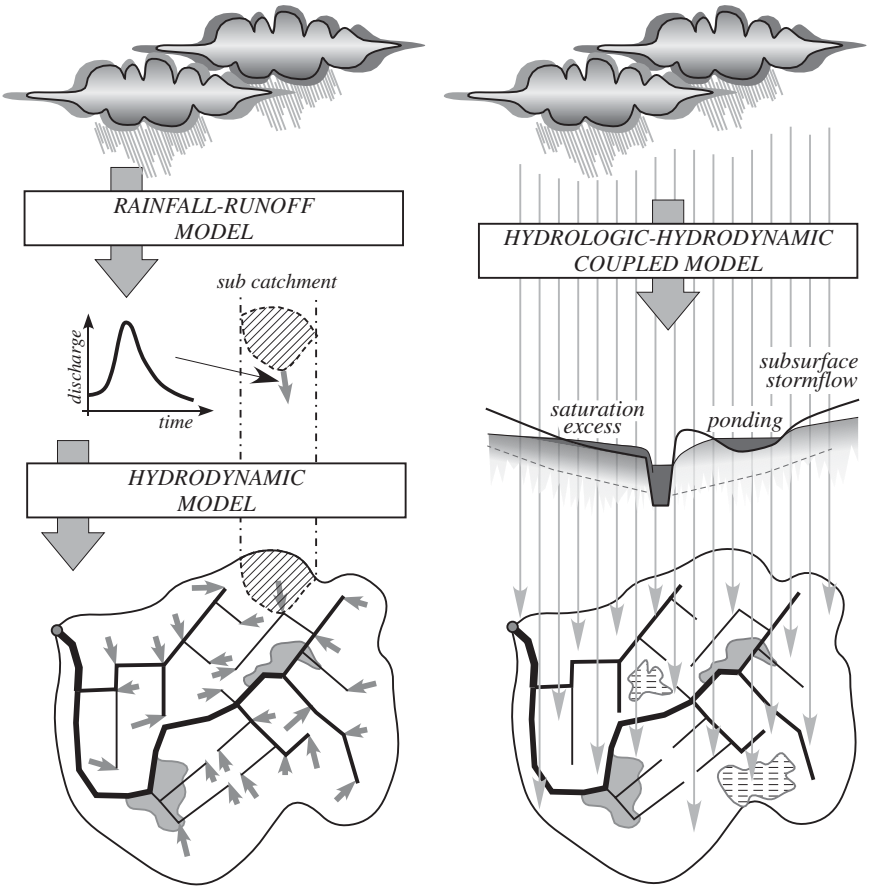

Figure 1. Schematic of alternative inundation model approaches: (left) the uncoupled approach versus (right) the coupled approach.

inefficiencies of the minor channel network (e.g., using conditional traveltime distributions [*Botter et al.*, 2010; *Benettin et al.*, 2013]). They can lead to a more accurate estimation of inflow hydrographs, but still the location of ponded areas cannot be predicted by the hydraulic model. In other words, the flooding of large, low-lying, or concave areas which are not (or inefficiently) drained cannot be predicted through the uncoupled approach. Further uncertainties arise from the choice of the number of segments into which each channel of the network should be subdivided, i.e., the number of subcatchments that should be used to maximize model accuracy. Also, the type of lateral inflow scheme (i.e., pointwise inflow at one end of each channel segment or uniformly distributed inflow along channel segments) to be used in order to accurately describe the actual inflow process is still an open issue [*Lerat et al.*, 2012].

A possible solution to the above problems is to use rainfall directly as boundary condition to the model (see Figure 1, right). This can be accomplished by employing suitable spatially distributed, physically based, coupled hydrological and hydraulic models. Such an approach is particularly attractive for the case of gently sloping, rural catchments, where the spatial organization of areas with different hydrological properties of the soil, the presence of linear landscape structures and their mutual interactions have been demonstrated to strongly affect the hydraulic connectivity and the surface runoff response of catchments [*Moussa et al.*, 2002; *Carluer and De Marsily*, 2004; *Ivanov et al.*, 2004; *Fiener et al.*, 2011; *Levavasseur et al.*, 2012; *Hallema et al.*, 2013].

Several models describing in a comprehensive manner atmospheric, surface, and subsurface processes and endowed with different degrees of complexity, accuracy, data requirements, and levels of coupling can be found in the literature [see e.g., *Morita and Yen*, 2002; *De Roo et al.*, 2003; *Furman*, 2008; *Camporese et al.*, 2010; *Borah*, 2011; *Nester et al.*, 2012]. The most complete and reliable models are typically adopted in small catchments characterized by nearly homogeneous conditions [e.g., *He et al.*, 2008]; however, in the last

decades, applications to large-scale watersheds to simulate the hydrological response have flourished in the literature [e.g., *Qu and Duffy*, 2007; *Li et al*., 2008; *Samaniego et al*., 2010; *Zhang et al*., 2010; *Kim et al*., 2012]. Also, many commercial or public domain models are available which are used worldwide and are being continuously developed (e.g., InHM [*VanderKwaak and Loague*, 2001], SWAT [*Arnold and Fohrer*, 2005], MIKE SHE [*Graham and Butts*, 2005], HydroGeoSphere [*Therrien et al*., 2005]). The objectives of such models are manifold and include (i) the prediction of midterm and long-term impacts of current management practices and alternative management policies; (ii) the prediction of impacts of future scenarios, e.g., related to the increasing anthropic pressure and climate changes; (iii) the improvement of our knowledge of large-scale, hydrologic processes; (iv) the reduction of overparameterization and the transferability of model parameters across scales and locations. In line with these objectives, such models mostly focus on groundwater flow and infiltration processes, which are often described in great detail by solving the 3-D Richards equation. They also include reliable and refined representation of the most relevant processes affecting the hydrologic budget, namely, canopy interception, evaporation, transpiration, snowmelt, exfiltration, or return flow. On the contrary, these models typically pay much less attention to the propagation of runoff, which actually plays the major role in inundation processes: overland flow is modeled using either the diffusive wave or the extended kinematic wave approximations of the 2-D shallow water equations (e.g., PAWS [*Shen and Phanikumar*, 2010] and PRMS [*Leavesley and Stannard*, 1995], respectively). The use of these equations implies sheet flow conceptualization of flow on a macroscale which is far from being a reliable approximation to the actual overland flow [e.g., *Carluer and De Marsily*, 2004; *Ivanov et al*., 2004; *Hallema et al*., 2013]. Accordingly, this type of models is not suitable to predict and to map with great accuracy the details of inundation from flood events.

To develop an integrated inundation model suitable for rural lowland catchments, specific needs have to be met. First, from a hydraulic viewpoint, the overland flow model must be able to describe the flow in the secondary drainage system, composed by the smaller ditches and furrows which are not explicitly resolved by the model. This capability is of primary importance for a reliable reconstruction of the volumes of water and flow rates actually entering the main channel network [*Defina*, 2000] and can be conveniently accomplished by using subgrid-scale modeling. Second, only the major hydrologic processes should be effectively described in order to reach a suitable compromise between realistic response and reliable applications [*Beven*, 1989; *Refsgaard*, 1997; *Hunter et al*., 2007].

With this in mind, here we propose the coupling of (i) a conceptual subsurface flow model which describes the relevant hydrologic processes occurring in the topsoil layer during heavy rainfall events; (ii) the overland flow model proposed by *Defina* [2000]. The latter is chosen because it provides a set of shallow water equations suitable to describe the dynamics of very shallow flows over irregular topography (rill flow), in which the ground surface is described not only through its elevation but includes a vertical length scale to account for small-scale (i.e., subgrid) topography.

The main advantages of the proposed integrated model, in comparison to the uncoupled approach, are (i) the identification of the subcatchments that drain to the main drainage channels, which often suffers from arbitrariness in lowland catchments, is not required; (ii) total rainfall rates can be directly applied as boundary condition: accordingly, rainfall-runoff models are not required to generate inflow hydrographs; (iii) the flooding due to the absence or the inefficiency of the minor drainage system composed of the smaller ditches can be effectively simulated.

The proposed 2-D model is described in section 2. Section 3 presents and discusses two real-world case studies aiming at providing information about the model capability in predicting flood generation and propagation, and inundation extent and pattern, rather than supporting a validation of the model.

2. The Integrated Mathematical Model

To construct the model we use the same procedure adopted by *Defina* [2000] to develop shallow water equations for a partially wet and topographically irregular ground surface. We then introduce a horizontal Representative Elementary Area (REA) and model the flow within this elementary domain. Since the REA has a size comparable to that of a computational element, then the model will describe the flow at the subgrid scale. A vertical cross section of the REA is shown in Figure 2.

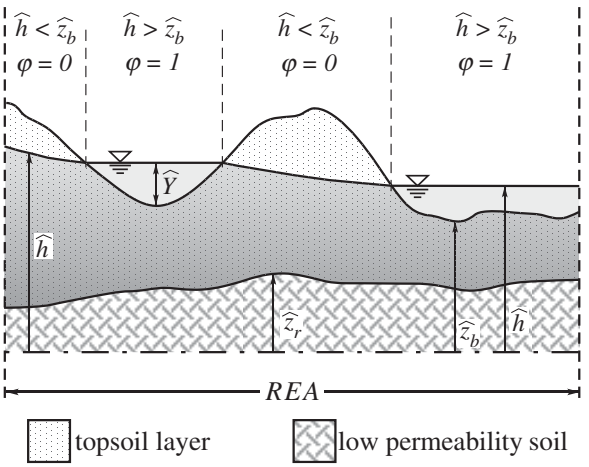

Figure 2. Representation of the flow field and bottom topography within the representative elementary area (REA), with notations.

Since most of the processes that control short-time response to intense rainfall events occur in the topmost part of the soil [*Burt and Slattery*, 1996; *Beven*, 2012], we introduce a topsoil layer of variable thickness to simulate the main hydrologic processes in the soil, i.e., rainfall infiltration, water storage and groundwater flow in the porous layer, and runoff production by the saturation excess mechanism. These processes are not described in great detail, e.g., by solving the saturated-unsaturated groundwater flow equations; we rather use a conceptual model to describe surface-subsurface flow interaction and the relevant processes in the topsoil layer. As a consequence, some parameters of this simple model lose their physical meaning and are conceptualized.

In the model we assume that the topsoil layer is characterized by high vertical infiltration (greater than the rainfall intensity) so that runoff is generated by the Dunne (i.e., saturation excess) mechanism. This is likely a reliable assumption because of tillage, typically required by most agricultural crops. Accordingly, we assume that rainfall immediately infiltrates into the shallow, possibly perched, saturated zone and flows down-gradient toward the draining channels.

Downward vertical percolation rate, through a lower permeability soil just below the topsoil layer, is also allowed. In this way, the Horton (i.e., infiltration excess) mechanism for runoff production can also be simulated by assuming a negligible thickness of the topsoil layer. The model thus contains a hybrid mechanism that incorporates both Horton and Dunne mechanisms [e.g., *Ivanov et al*., 2004; *Slattery et al*., 2006; *Loague et al*., 2010].

The topsoil porous layer is treated as a confined aquifer where water ponds on the ground surface and as an unconfined aquifer elsewhere. Darcy's law and the Dupuit-Forchheimer assumption are used to solve for the 2-D flow in the topsoil porous layer. With these assumptions, water elevation $\hat{h}$ describes a continuous surface, lying either above or below the ground surface (Figure 2).

2.1. The Model Equations

The mass balance equation at a point within the REA for overland and subsurface flow can be written as

$$\frac{\partial \hat{w}_s}{\partial t} + \nabla \cdot \hat{\mathbf{q}}_s + \varphi(\hat{s} - \hat{r}) = 0 \tag{1}$$

$$\frac{\partial \hat{w}_f}{\partial t} + \nabla \cdot \hat{\mathbf{q}}_f - (1-\varphi)\hat{r} - \varphi\hat{s} + \hat{f} = 0 \tag{2}$$

where t denotes time, $\hat{w}_s$ is the volume of water per unit area ponding the ground, $\hat{w}_f$ is the volume of water per unit area stored in the topsoil layer, $\nabla\cdot$is the two-dimensional divergence operator, $\hat{\mathbf{q}}_s = (\hat{q}_{sx}, \hat{q}_{sy})$ and $\hat{\mathbf{q}}_f = (\hat{q}_{fx}, \hat{q}_{fy})$ are the surface and subsurface flow rate per unit width, respectively, $\hat{r}$ is the rainfall rate, $\hat{s}$ is the infiltration rate from the wetted fraction of the REA into the topsoil layer, $\hat{f}$ is the downward vertical percolation rate, $\varphi(x, y, t)$ is the superficial phase function defined such that $\varphi = 1$ if $\hat{h} > \hat{z}_b$ and $\varphi = 0$ elsewhere, $\hat{h}$ being the water elevation (either above or below the ground surface) and $\hat{z}_b$ the ground surface elevation (see Figure 2).

Combining equations (1) and (2) yields

$$\frac{\partial \hat{w}}{\partial t}+\nabla\cdot\hat{\mathbf{q}}-\hat{r}+\hat{f}=0 \tag{3}$$

where $\hat{w}$ is the volume of water per unit area stored in the REA and $\hat{\mathbf{q}}=\hat{\mathbf{q}}_s+\hat{\mathbf{q}}_f$ is the total flow rate per unit width.

The volume of water per unit area stored at a point can be written as

$$\hat{w}=\varphi(\hat{h}-\hat{z}_b)+\varphi\hat{n}_e(\hat{z}_b-\hat{z}_r)+(1-\varphi)\hat{n}_e(\hat{h}-\hat{z}_r) \tag{4}$$

where $\hat{n}_e$ is the effective porosity and $\hat{z}_r$ the elevation of the quasi-impervious bottom of the topsoil layer.

Since $\partial\hat{z}_b/\partial t=\partial\hat{z}_r/\partial t=0$, substitution of equation (4) into the mass balance equation yields

$$[\varphi+\hat{n}_e(1-\varphi)]\frac{\partial\hat{h}}{\partial t}+\nabla\cdot\hat{\mathbf{q}}-\hat{r}+\hat{f}=0. \tag{5}$$

Equation (5) is then averaged over the REA, and averaged variables are denoted without the hat. Both the effective porosity $\hat{n}_e$ and the source terms $\hat{r}$ and $\hat{f}$ can reasonably be assumed constant within the REA (i.e., $\hat{n}_e=n_e,\hat{r}=r,\hat{f}=f$). Free surface elevation $\hat{h}$ is assumed to vary smoothly throughout the whole domain, so that it can be assumed approximately constant within the REA (i.e., $\hat{h}=h$). With these assumptions and recalling that the averaging procedures satisfies the Gauss' rule, equation (5) averaged over the REA can be written as

$$\vartheta(h)\frac{\partial h}{\partial t}+\nabla\cdot\mathbf{q}-r+f=0 \tag{6}$$

where $\vartheta(h)=\eta(h)+n_e[1-\eta(h)]$ can be interpreted as an h-dependent storativity coefficient, with $\eta(h)=(1/A)\int_A\varphi dA$ the wet fraction of the REA. According to *Defina* [2000], the function $\eta(h)$ can be expressed as

$$\eta(h)=\frac{1}{2}\{1+\mathrm{erf}\,[2(h-z_b)/a_r]\} \tag{7}$$

where $\mathrm{erf}(\cdot)$ is the error function and a_r the height of ground irregularities which can be approximated as twice the standard deviation of ground elevation, $\hat{z}_b$, within the REA (further details about the parameter a_r are given in section 3; the reader is also referred to *Defina* [2000, 2003] and *D'Alpaos and Defina* [2007]).

The downward vertical percolation rate f in equation (6) can be estimated with any infiltration model, e.g., the Green-Ampt model.

As stated in section 1, momentum equations for overland flow over irregular and partially dry ground surface were proposed by *Defina* [2000] who adopted the same averaging procedure over a REA we use in the present work. These equations can be written as

$$\nabla h+\frac{1}{g}\frac{\mathrm{d}}{\mathrm{d}t}\left(\frac{\mathbf{q}_s}{Y}\right)+\frac{\tau_b}{\rho gY}=0 \tag{8}$$

where the local and advective accelerations are lumped into one term, i.e., the total time derivative of the depth integrated velocity $\mathbf{q}_s/Y$ [see e.g., *Walters and Casulli*, 1998; *Giraldo*, 2000; *Defina*, 2003], g is gravity, $\tau_b=(\tau_{bx},\tau_{by})$ is the bed shear stress, and Y the equivalent water depth, defined as the volume of water per unit area actually ponding the ground. The latter is given as [*Defina*, 2000]

$$Y=a_r\left\{\eta(h)+\frac{1}{4\sqrt{\pi}}\exp\left[-4\left(\frac{h-z_b}{a_r}\right)^2\right]\right\}. \tag{9}$$

The flow in the saturated portion of the porous layer is governed by the Darcy's law and can be effectively modeled by assuming the Dupuit-Forchheimer approximation. As shown in Figure 2, if $\hat{h}>\hat{z}_b$ (i.e., water is

ponding on the ground), the porous layer behaves as a confined aquifer with thickness $\hat{z}_b - \hat{z}_r$; on the contrary, if $\hat{h} < \hat{z}_b$ the aquifer, with thickness $\hat{h} - \hat{z}_r$, is unconfined. We then can write

$$\hat{\mathbf{q}}_f = -\varphi K(\hat{z}_b - \hat{z}_r)\nabla\hat{h} - (1-\varphi)K(\hat{h} - \hat{z}_r)\nabla\hat{h} \tag{10}$$

where K is the horizontal saturated hydraulic conductivity which is assumed to be constant within the REA. The averaging of equation (10) over the REA gives

$$\mathbf{q}_f = -K(h - z_r - Y)\nabla h. \tag{11}$$

Equations (6), (8), and (11) provide the two-dimensional, coupled surface-subsurface flow model.

In the numerical solution of model equations we can assume that the REA corresponds to the generic computational cell. The proposed model assumes that both types of flow, i.e., free surface flow over confined groundwater flow and unconfined groundwater flow, coexist at each point in the domain (i.e., within each computational cell); the function η provides the fraction of wet area where the first type of flow occurs, whereas $1 - \eta$ provides the fraction of dry area where the second type of flow occurs. Accordingly, the model can predict a partially wet state in each computational cell, e.g., the presence of ditches filled with water and small puddles within a dry area. The presence of subgrid features, such as small furrows, ditches, and bumps, are accounted for in the model through the parameter a_r, which measures the deviation of ground elevation from a (piecewise) planar surface [*Defina*, 2000].

The procedure used here to couple the surface and subsurface flows is similar to the one proposed by *Liang et al*. [2007] and by *Yuan et al*. [2008] and later improved [*Kong et al*., 2010; *Eck et al*., 2012]. However, the present model assumes that different states coexist within a single computational cell, whereas the model proposed by *Liang et al*. [2007] and by *Yuan et al*. [2008] assumes that each computational cell can be either wet or dry. Accordingly, subgrid features (e.g., the flow through the smaller ditches) cannot be described by the latter model. Our model shares some similarities with the model proposed by *Defina and Matticchio* [1994]. Unlike *Liang et al*. [2007] and *Defina and Matticchio* [1994]; however, our model allows rainfall to be imposed as a boundary condition, which is actually one of the main aims of the present contribution.

2.2. The Numerical Model

The solution to the above set of equations does not require a specific numerical technique and different computational methods can be used; in the following we shortly describe the numerical model we use in the simulations presented and discussed in section 3.

Momentum equation for overland flow (8) can be averaged over the computational time step, Δt, and linearized to yield (see *Defina* [2003] for details)

$$\mathbf{q}_s = -\Psi_s \nabla h + \Phi_s \tag{12}$$

where

$$\Psi_s = \left[\frac{1}{gY\Delta t} + \frac{|\mathbf{q}_s|}{n^2 \cdot H^{10/3}}\right]^{-1} \tag{13}$$

$$\Phi_s = -\left[\frac{1}{gY\Delta t}\left(\frac{\mathbf{q}_s}{Y}\right)_0\right]\Psi_s. \tag{14}$$

In equation (13), $H = Y + 0.27 a_r \sqrt{Y/a_r}\exp(-2Y/a_r)$ is an equivalent water depth [*Defina*, 2000] and n is the Manning's roughness coefficient. In equation (14), $(\mathbf{q}_s/Y)_0$ denotes the velocity vector at the previous time step and at the departure point, i.e., the position of a fluid particle at the previous time step along the

Lagrangian trajectory [*Defina*, 2003]. Both Ψ_s and $\mathbf{\Phi}_s=(\Phi_{sx},\Phi_{sy})$ are computed at previous time step under the assumption of slowly varying flow.

Combining equations (10) and (12), the total flow rate **q** can be written as

$$\mathbf{q}=-(\Psi_s+\Psi_f)\nabla h+\Phi_s \tag{15}$$

where $\Psi_f=K(h-z_r-Y)$ is computed at previous time step. Equation (6) with equation (15) gives

$$\vartheta(h)\frac{\partial h}{\partial t}-\nabla\cdot[(\Psi_s+\Psi_f)\nabla h]+\nabla\cdot\Phi_s-r+f=0. \tag{16}$$

Equation (16) for the free surface elevation *h* is solved with a semi-implicit, staggered finite element Galerkin's method. At each time step, flow rates $\mathbf{q}_s$ and $\mathbf{q}_f$ are then computed by back substitution of *h* into equations (12) and (11), respectively.

In the examples discussed in section 3 the model also uses one-dimensional (1-D) open channel elements to describe the flow in the channels dissecting the lowland basins, and 1-D links which are 1-D elements describing, e.g., the flow under sluice gates or over weirs, levees, and other embankments, the flow through pipes, and the operation of pumping stations controlled by upstream water level. The way in which 1-D contribution is included in the model is detailed in *Martini et al*. [2004], *D'Alpaos and Defina* [2007], and *Viero et al*. [2013].

The capability of the hydrodynamic model to efficiently reproduce the overland flow, as well as the flow routing via both 1-D and 2-D elements, have been demonstrated by, e.g., *Defina* [2000], *Martini et al*. [2004], *D'Alpaos and Defina* [2007], and *Viero et al*. [2013]. The effectiveness of the coupling technique and the ability of the coupled model to reproduce the overall rainfall-runoff process are yet to be proved: this issue is addressed in section 3.

3. Model Applications

The model was applied to simulate flood events in two rural lowland catchments located South of Venice, in the North-East of Italy: the Rebosola catchment and the Sadocca catchment. We choose these two lowland catchments because (i) inflows from the neighboring catchments are negligible; therefore, from the hydrological point of view, the catchment boundaries can unambiguously be determined; (ii) enough and accurate enough hydrologic and topographic data are available and allow for a meaningful comparison between measured and computed flow rates and water levels; (iii) surveyed areas which were flooded during recent storm events are also available to be compared with model predictions [*Sebben et al*., 2012]; (iv) the land use in both the catchments is almost entirely agricultural, characterized by a surface drainage system (i.e., drained by surface ditches and not by subsurface drains which are not included in the model); and (v) the densely populated fraction of the catchments is small; therefore, the impact of the pipe drainage systems, which is not included in the model, is generally negligible.

To construct the models we used ground elevations extracted from technical maps having a mean horizontal resolution of approximately 100 m, with a few, more densely arranged surveyed points in the neighborhood of topographic discontinuities. The topography of the main channels was also available, being provided by the Land Reclamation Authorities.

3.1. Boundary and Initial Conditions

Hourly data of uniformly distributed gross rainfall were applied to the whole computational domain. The downstream boundary condition in both the catchments is provided by the pumping stations (reproduced via 1-D links) which pump the water out of the domain according to prescribed activation/deactivation water levels.

In order to prescribe reliable initial conditions to the system, we determined the maximum time required by the catchment to reach stationary flow when forced with constant boundary conditions. We forced the initially dry catchment with a constant rainfall having a rate corresponding to the pumping station capacity.

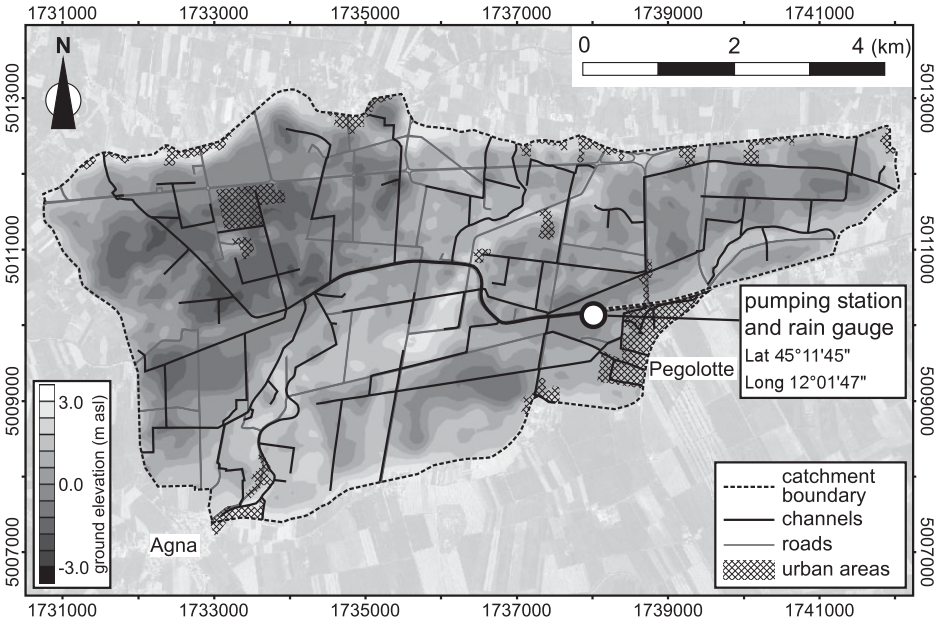

Figure 3. Gray-scale elevation map of the Rebosola catchment with the location of the pumping station and rain gauge. The main channel network (black continuous lines), the main roads (gray lines), and the urban areas (hatched areas) are also reported. Coordinates are in EPSG 3003.

When steady flow conditions were attained, we stopped the rainfall and measured the time, T, required by the catchment to recover fully dry conditions: T can be interpreted as the hydrologic memory of the catchment. It can be reasonably assumed that a single storm event is negligibly affected by rainfall that occurred T or more days before. Accordingly, we started real event simulations at $t=-2T$ with respect to the beginning of each storm event with arbitrary initial conditions and discarded the results computed in the time interval from $t=-2T$ to $t=0$ since they were likely affected by the arbitrarily imposed initial conditions.

3.2. Sensitivity Analysis and Model Parameters

To be consistent with the degree of conceptualization of the subsurface model and in order to avoid overparameterization, in the model applications a constant percolation rate $f=f_0$ was assumed when $h > z_r$, otherwise $f=0$. A constant depth, D, of the topsoil layer was also assumed, so that $z_r=z_b-D$, which is consistent with the idea of, e.g., nearly constant tillage depth typical of agricultural soils.

A preliminary sensitivity analysis showed that the porous layer thickness, D, and the effective porosity, n_e, mainly control the surface runoff volume and the time at which runoff production starts. The product $(n_e \cdot D)$ gives the maximum volume of water per unit area which can be stored in the topsoil layer: the greater the volume, the smaller the runoff production. The vertical percolation rate, f, and the topsoil hydraulic conductivity, K, have a significant impact on the outflow hydrographs since these parameters mainly control the state of the catchment at the beginning of a storm event and the overall runoff coefficient. This peculiarity of the parameters allowed us to perform a robust calibration of the subsurface model in real-world applications.

With regard to the hydrodynamic parameters, the height of topographic features or macroroughness, a_r, mainly affects the wetting and drying process. Small a_r causes a sharp wet-dry transition when the free-surface elevation is close to the mean bottom elevation of the computational cells; conversely, large values of a_r determine a smoother transition. The parameter a_r and the Manning friction coefficient n control the propagation of the free surface flow and, due to the subgrid model, also affects the shape of the outflow hydrograph. Nevertheless, both a_r and n are essentially hydrodynamic parameters, to be set in order to correctly simulate the flooding dynamics rather than the rainfall-runoff process.

Table 1. Pump Activation (h_{ON}) and Deactivation (h_{OFF}) Levels for the Rebosola Pumping Station

Pump	Discharge (m^3/s)	h_{ON} (m asl)	h_{OFF} (m asl)
G_1	2.0	−2.50	−2.61
G_2	2.0	−2.41	−2.58
G_3	2.0	−2.33	−2.55
G_4	3.0	−2.25	−2.52

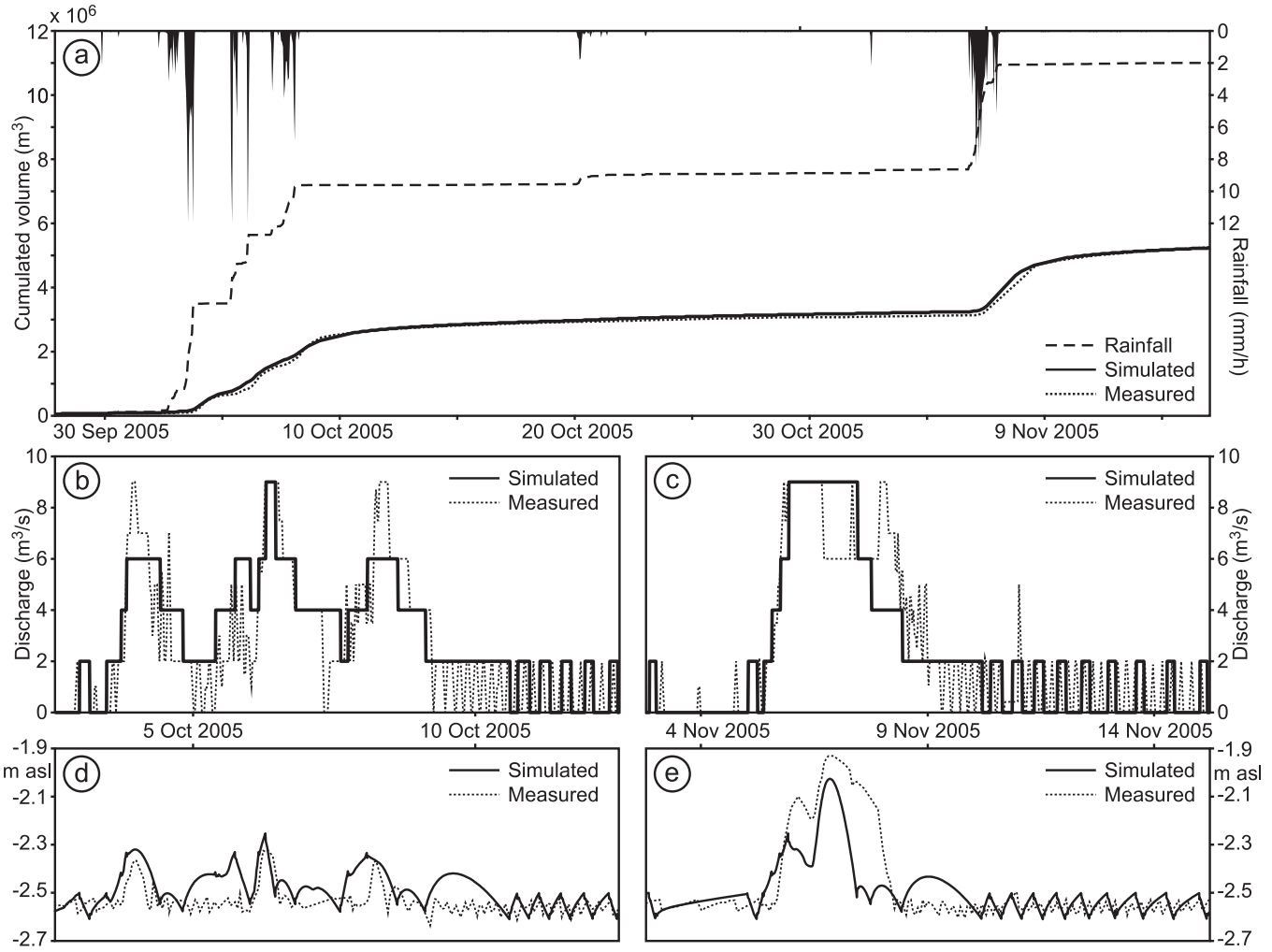

Figure 4. Comparison between model results and measured data for two consecutive events occurred in the Rebosola catchment in Autumn 2005: (a) rainfall intensity (right scale) and cumulative volumes of rainfall (dashed line), of measured runoff (gray line), and computed runoff (black line); (b) measured (dotted line) and computed runoff (black line) at the catchment outlet for the storm event of October 2005; (c) same as Figure 4b for the storm event of November 2005; (d) measured (dotted line) and computed (black line) water level at the pumping station for the storm event of October 2005; (e) same as Figure 4d for the storm event of November 2005.

3.3. Model Calibration

Different calibration techniques have been proposed in the literature, to effectively deal with overparameterization, spatial heterogeneities, and the transferability of model parameters across scales and locations [see e.g., *Samaniego et al.*, 2010, and references therein]. In the present model application, given the limited size of the considered catchments (area $<10^2$ km^2) and the specific aim and preliminarily nature of the study, a simple parameterization technique has been applied which is based on the "hydrological response units" (HRUs) [*Kumar et al.*, 2013]. Four HRUs have been identified: cultivated terrains, roads, paved areas, and channels (see Figures 3 and 7). Computational elements belonging to homogeneous regions are grouped into HRUs, and a unique set of model parameters is defined for each HRU. A simple trial and error procedure was used to calibrate the model. As a result, the obtained parameterization is valid only for the scale on which the model is calibrated.

Table 2. The Rebosola Case Study[a]

Size of the Averaging Window (h)	RMSE (m^3/s)	NSE	R^2
1	0.96	0.74	0.76
2	0.87	0.78	0.80
4	0.75	0.83	0.84
6	0.68	0.86	0.87
8	0.62	0.88	0.89

[a]Quantitative comparison of measured and modeled pumped discharges.

Seven significant storm events in the period 2004–2011 were available for the Rebosola

Table 3. The Rebosola Case Study[a]

Size of the Averaging Window (h)	RMSE (m)	NSE	R^2
1	0.065	0.42	0.45
2	0.062	0.45	0.48
4	0.060	0.48	0.50
6	0.059	0.50	0.52
8	0.057	0.52	0.54

[a]Quantitative comparison of measured and modeled water levels close to the pump station.

catchment, and four events in the period 2008–2010 were available for the Sadocca catchment. We used most of the available flood events to calibrate the model. The aim of the present study is not to develop a predictive tool for the catchments at hand, but it is rather to investigate if the model structure inherently has the capability of describing the overall hydrologic processes which include runoff production, flood propagation, and land flooding. Accordingly, only one storm event among the available for each catchment was excluded from the calibration data set and used for validation purposes.

In both the applications, the height of topographic features or macroroughness, a_r, was set equal to 0.3 m, based on topographic studies that we performed in similar lowland catchments for which refined LiDAR data were available. The following values for the Manning friction coefficient were selected based on our experience: $n=0.033\,\mathrm{sm}^{-1/3}$ for cultivated terrains, $n=0.025\,\mathrm{sm}^{-1/3}$ for roads and paved areas, and $n=0.028\mathrm{sm}^{-1/3}$ for channels.

The limited geotechnical information and the high degree of conceptualization of the subsurface model have lead us to consider the topsoil layer depth, D, the horizontal hydraulic conductivity, K, the vertical percolation rate, f_0, and the effective porosity, n_e, as calibration parameters.

In the urban fraction of the catchments, the thickness of the porous layer was arbitrarily set to a negligibly small value ($D=2$ cm) and a small vertical percolation rate ($f_0=0.001$ mm/h) was assumed to simulate nearly impervious ground surface condition. In this way, the Horton (i.e., infiltration excess) mechanism for runoff production was simulated. In the rural fraction of the catchments, the thickness of the porous layer was set to $D=0.5$ m, slightly deeper than the typical tillage depth. The horizontal hydraulic conductivity was set to a relatively high value ($K=0.001$ m/s), accounting for the effect of tillage; the effective porosity, n_e, was set to 0.25. To calibrate the vertical percolation rate, f_0, in the rural fraction of the catchments we focused on short periods having two successive rainfall events so that the runoff produced by the second rainfall event was largely affected by the water content in the topsoil layer, hence by f_0. We found $f_0 \approx 0.35$ mm/h and $f_0 \approx 0.06$ mm/h for the Rebosola and Sadocca catchment, respectively. With these model parameters, the time T (i.e., hydrologic memory of the catchment, previously described) was found to be approximately $T=15$days for the Rebosola catchment and $T=20$ days for the Sadocca catchment.

3.4. The Rebosola Case Study

The Rebosola catchment (Figure 3) covers an area of approximately 37.5 km^2 with the ground elevation in the range from −3 to 3masl. The urban areas are mainly located along the boundaries of the catchment (dashed areas in Figure 3). The model domain is described by a mesh composed by approximately 12,000 nodes, 23,600 triangular elements, 1400 1-D channel elements, and one 1-D link to simulate the operation of the pumping station; the average area of triangular elements is approximately 1600m^2. The downstream boundary condition is provided by one pumping station whose operation is controlled by water level according to the activation/deactivation levels given in Table 1. The pumping station has a capacity of 9 m^3/s. Hourly rainfall data were recorded at a rain gauge located nearby the Rebosola pumping station (Lat 45°11′45″, Long 12°01′47″) and operated by the "Adige-

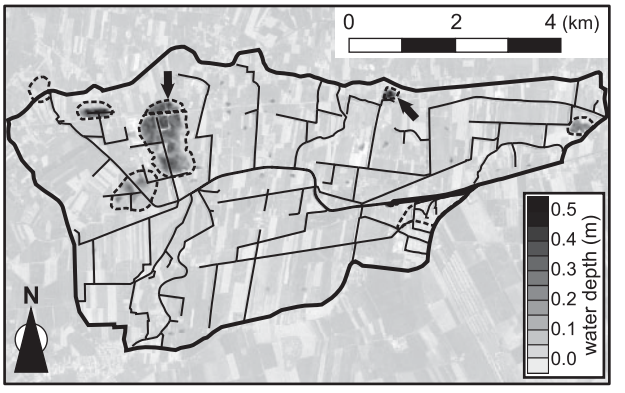

Figure 5. The Rebosola case study. Surveyed (black dashed line) and simulated (gray scale) flooded areas during the storm event of November 2005. Black arrows indicate the areas that are flooded because of inefficiency of the minor drainage network composed of the smaller ditches.

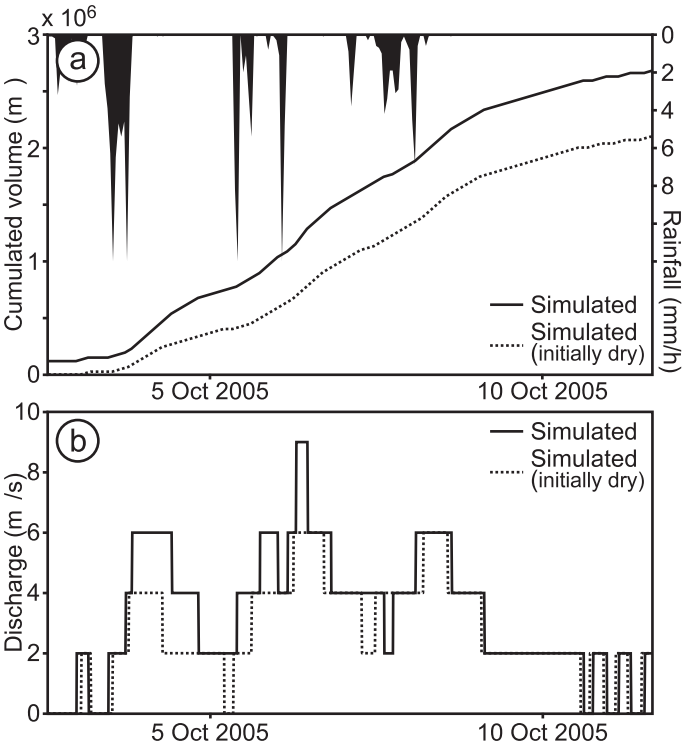

Figure 6. Storm event of October 2005 occurred in the Rebosola catchment: (a) comparisons between the cumulative volume predicted by the model when initial conditions are those determined by the model itself (black line) with that computed when fully dry initial conditions are prescribed (dotted line); (b) same as Figure 6a when pumped flow rates are compared.

Euganeo" Land Reclamation Authority. Discharges and water levels at the pumping station were recorded by the monitoring and control system of the above Land Reclamation Authority with a temporal resolution of 15 min.

Figure 4 compares model prediction with measured data for two consecutive storm events which occurred in the period October–November 2005 (the second storm event, which occurred in the early November, was excluded from the calibration data set). Measured and simulated runoff cumulative volumes over the whole period are compared in Figure 4a and show a good agreement (RMSE$=0.076 \cdot 10^6$ m^3, Nash-Sutcliffe efficiency NSE$=0.998$, $R^2=0.999$). The comparison between computed and measured pumped outflow rate (Figures 4b and 4c) and water levels close upstream of the pumping station (Figures 4d and 4e) shows a less good, but still acceptable agreement. It is worth saying that small errors in the prediction of water level can produce rather different pump activation/deactivation time sequences and, consequently, different time behaviors of water levels and discharges. Moreover, close inspection of measured data shows that, during these storm events, some manual alterations to pumps on/off settings have occurred: e.g., during the first storm event the four pumps were all activated even when water level remained below -2.3 masl, and during the second event pump G_4 was turned off although water level was well above -2.5 masl. For these reasons, a quantitative comparison between instantaneous computed and measured water levels and flow rates close to the pumping station is weakly significant. In order to deal with the above shortcoming, we low-pass filtered discharges and water levels (both measured and observed) through a moving average operation, thus reducing short-term fluctuations. The performance indexes, computed for moving windows of different sizes, are given in Tables 2 and 3. Note that the averaging windows are much shorter than flood duration. The improvement of performance indexes with increasing the size of the averaging window points out the great impact of pumps' activation/deactivation on discharges and water levels close to the pumping station.

Figure 5 compares surveyed and simulated inundated areas, showing a generally good agreement. Importantly, close inspection of the numerical results shows that for some of the flooded areas (indicated with an arrow in Figure 5) the water ponding on the ground does not come from the modeled channels, demonstrating that inundation is due to inefficiencies of the minor drainage network (i.e., small furrows not explicitly modeled) rather than to insufficient channel conveyance capacity.

To show the impact of the initial conditions on runoff volumes and discharges, the model was run to reconstruct the storm event of October 2005 starting from fully dry catchment condition. The results of this simulation are shown in Figure 6: Figure 6a compares the cumulative volume predicted by the model when initial conditions are those determined by the model itself with that computed when fully dry initial conditions are prescribed; Figure 6b shows the same comparison for the pumped discharge. The impact of the catchment state at the beginning of the storm event is actually large; e.g., runoff volumes,

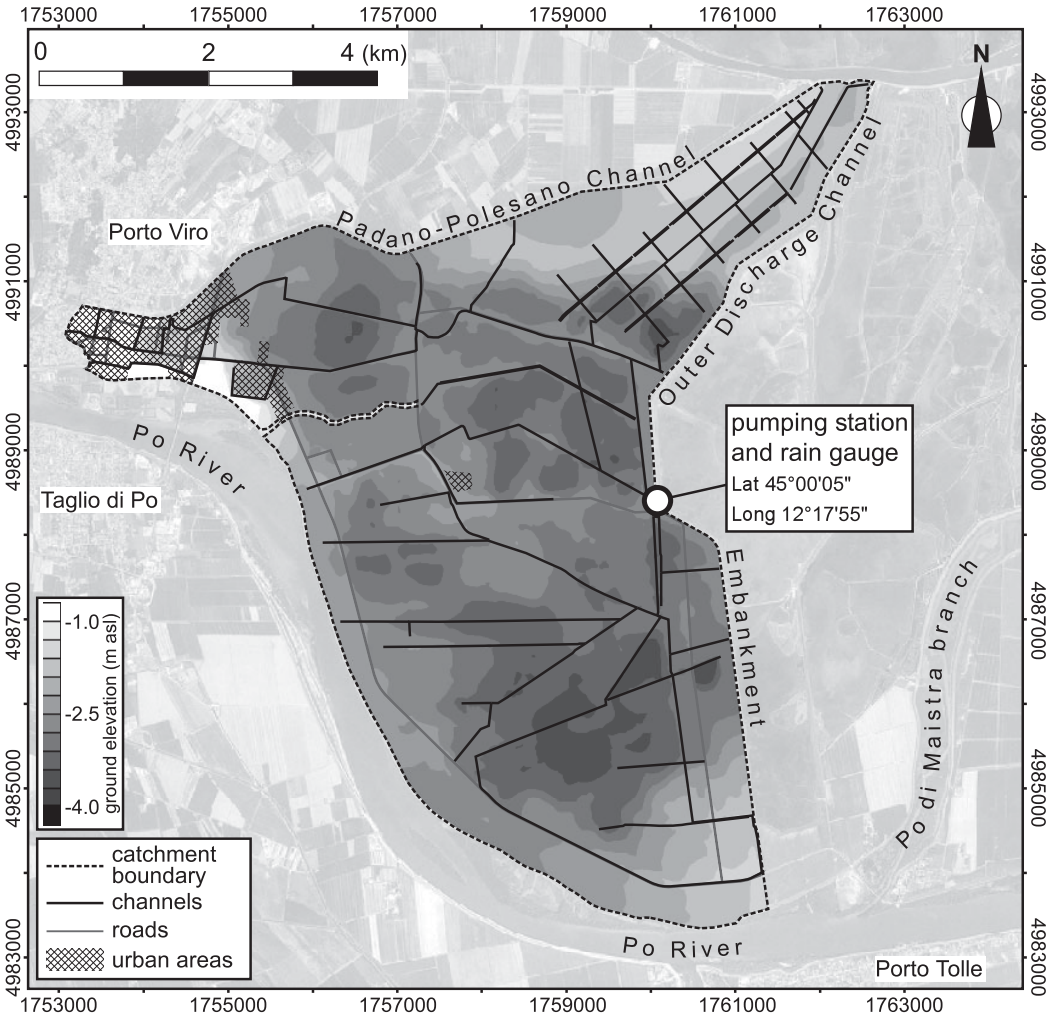

Figure 7. Gray-scale elevation map of the Sadocca catchment with the location of the pumping station and rain gauge. The main channel network (black continuous lines), the main roads (gray lines), and the urban areas (hatched areas) are also reported. Coordinates are in EPSG 3003.

computed with the different initial conditions, differ by 22% at the end of the simulation period (11 October, 12:00 noon).

3.5. The Sadocca Case Study

The Sadocca catchment (Figure 7) has an area of approximately 41.0 km^2, it is bounded by the Po River to the South-West, by the Padano-Polesano Channel to the North and, to the East, by the Outer Discharge Channel, North to the pumping station, and by a massive embankment separating the catchment from a fishery farming area in the Po River Delta Natural Reserve, South to the pumping station. Ground elevation in the catchment ranges from −4 to 0masl. The domain is described by a mesh composed by approximately 17,600 nodes, 34,800 triangular elements, 2300 1-D channel elements, and one 1-D link to simulate the operation of the pumping station; the average area of triangular elements is approximately 1200m^2. As for the Rebosola case study, the downstream boundary condition is provided by one pumping station whose operation is controlled by water level according to the activation/deactivation levels given in Table 4. The pumping station has a

Table 4. Pump Activation (h_{ON}) and Deactivation (h_{OFF}) Levels for the Sadocca Pumping Station

Pump	Discharge (m^3/s)	h_{ON} (m asl)	h_{OFF} (m asl)
G_1	3.0	−4.00	−4.20
G_2	3.0	−3.90	−4.15
G_3	2.0	−3.80	−4.10
G_4	2.0	−3.70	−4.00
G_5	2.0	−3.60	−3.90

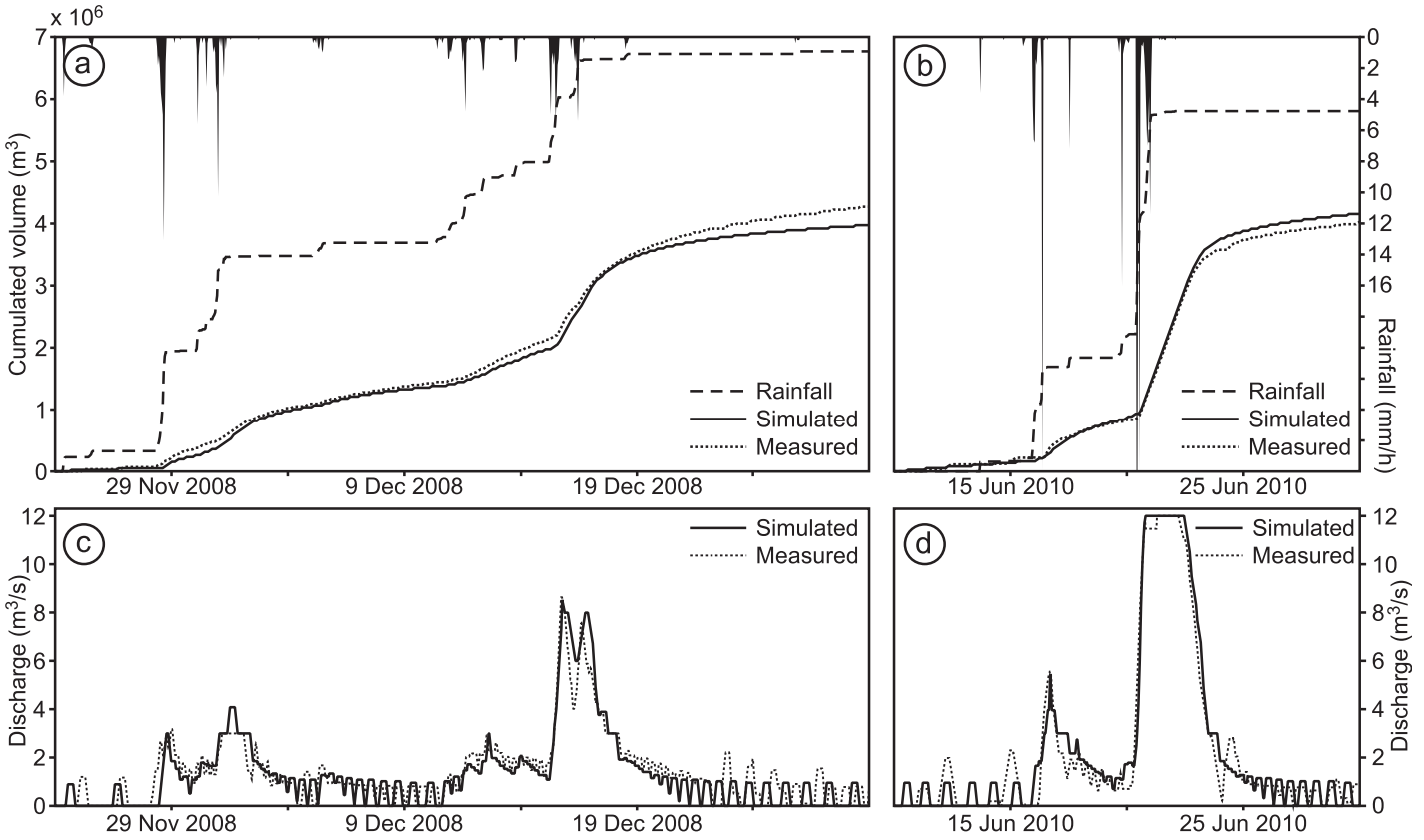

Figure 8. The Sadocca case study. Left panels refer to the storm event occurred in December 2008, and right panels refer to that of June 2010. Upper panels show rainfall intensity, cumulated rainfall volume (dashed line), and measured (dotted line) and simulated (black line) runoff volumes. Lower panels compare measured (dotted line) and simulated (black line) runoff rates. Note that, given the relatively high frequency of pumps activation and deactivation, and in order to improve figure readability, discharges in Figures 8c and 8d were averaged over a moving window of 8 h.

capacity of $12 m^3/s$. Hourly rainfall data were recorded by a rain gauge located close to the pumping station (Lat 45°00′05″, Long 12°17′55″) and operated by the "Delta del Po" Land Reclamation Authority. Pumped runoff to the Outer Discharge Channel was recorded by the monitoring and control system managed by the above Land Reclamation Authority with a temporal resolution of 5 min. Water level at the pumping station was not available.

For the Sadocca case study we present results for two storm events. The first storm was used in the calibration data set, whereas the second was used as a validation event. The simulation of the first event was run from 1 October to 31 December 2008 and model results computed before 24 November were discarded being affected by the arbitrarily prescribed initial conditions. The simulation of the second event was run from 20 April to 1 July 2010, and the results from 10 June were retained for comparison with measured data.

Table 5. The Sadocca Case Study[a]

Size of the Averaging Window (h)	RMSE (m^3/s)	NSE	R^2
1	1.57	0.20	0.38
2	1.41	0.29	0.45
4	1.06	0.51	0.61
6	0.79	0.70	0.76
8	0.64	0.79	0.83

[a]December 2008 storm event: quantitative comparison of measured and modeled pumped discharges.

Figures 8a and 8b show the observed rainfall rate and rainfall cumulative volume. Measured and simulated cumulative pumped volumes (Figures 8a and 8b) show a generally good agreement ($RMSE = 0.147 \cdot 10^6\ m^3$, $NSE = 0.991$, $R^2 = 0.998$ for the December 2008 event; $RMSE = 0.099 \cdot 10^6\ m^3$, $NSE = 0.997$, $R^2 = 0.999$ for the June 2010 event), although the model predicts a recession phase that is shorter in time when compared to the surveyed one for the winter event. The agreement between observed and simulated discharges is also rather good (Figures 8c and 8d). As for the Rebosola

Table 6. The Sadocca Case Study[a]

Size of the Averaging Window (h)	RMSE (m^3/s)	NSE	R^2
1	1.65	0.80	0.81
2	1.60	0.83	0.84
4	1.21	0.89	0.89
6	0.98	0.92	0.93
8	0.83	0.94	0.94

[a]June 2010 storm event: quantitative comparison of measured and modeled pumped discharges.

Table 7. Urban Areas in the Rebosola and Sadocca Catchments[a]

	A (km^2)	A_{urb} (km^2)	A_{urb}/A(%)
Rebosola	37.5	2.4	6.5
Sadocca	41.0	1.7	4.1

[a]A is the catchment area and A_{urb} is the urban area.

case study, we computed performance indexes after averaging discharge time series (both measured and observed) over moving windows of different sizes which, however, are much shorter than the flood duration. Results are given in Tables 5 and 6 and confirm the great impact of pumps' activation/deactivation on discharges at the pumping station.

Water level at the pumping stations were not available and no comparison with model prediction could be made. Also, no information about flooded areas was available for the storm events which occurred in the Sadocca catchment during the observation period.

3.6. The Impact of Urban, Impervious Areas

In order to show the impact of urban (i.e., impervious) areas on the hydrological response to storm events, two further simulations were performed by replacing urban areas with rural areas all over both the Rebosola and Sadocca catchments.

As summarized in Table 7, the Rebosola catchment has a slightly larger fraction of urban area (6.5%) with respect to the Sadocca catchment (4.1%). In addition, the larger urban area in the Rebosola catchment, i.e., Pegolotte town (Figure 3) is located close to the pump station. This circumstance is likely to produce more significant impact on the hydrological response if compared to the case of Sadocca catchment, where the urban area is relatively small and located far from the outlet (i.e., Porto Viro town, see Figure 7).

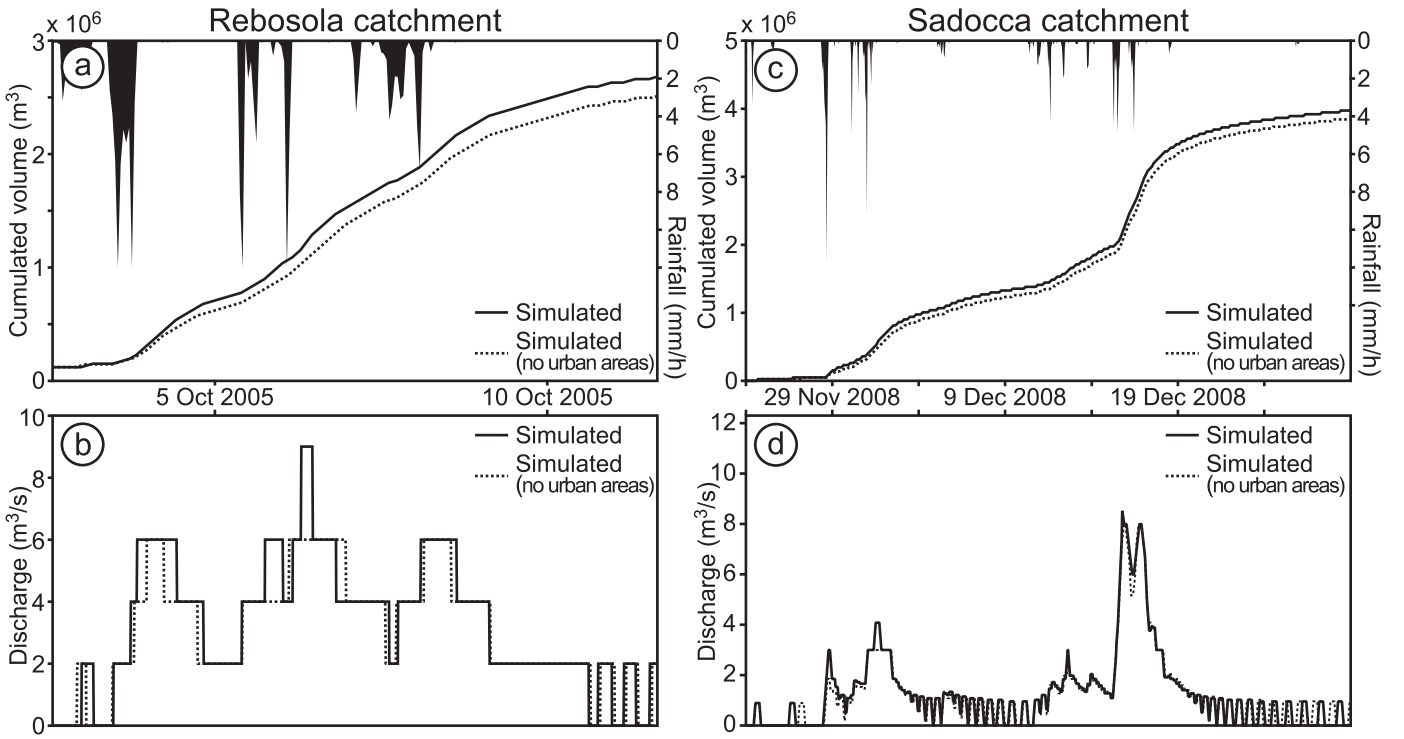

Figure 9. The impact of urban, impervious areas: (a) rainfall intensity (storm event of October 2005) and cumulative runoff volumes computed when considering the urban, impervious areas of the Sadocca catchment (solid line) and after replacing urban with agricultural areas (dotted line); (b) runoff discharges in the presence (full line) and absence (dotted line) of urban areas in the Rebosola catchment (storm event of October 2005); (c) and (d) same as Figures 9a and 9b for the storm event of December 2008 occurred in the Sadocca catchment.

The results of this investigation are shown in Figure 9 where the pumped cumulative volume and discharge computed by assuming impervious and pervious surface for the urban areas are compared.

When urban areas are replaced with rural areas, the computed runoff volume reduces. Interestingly, runoff volume reduction is approximately 7% for the Rebosola catchment where 6.5% of the total area is urbanized and approximately 3% for the Sadocca catchment where 4.1% of the total area is urbanized.

Runoff volume reduction is the highest at the beginning of a rainfall event, because of the larger water volumes that can be stored in the ground. Accordingly, it is the early runoff discharge which reduces with respect to the case of impervious ground surface, whereas, with the progress of time, the topsoil layer saturate and runoff turns out to be comparable to that from impervious surface (Figures 9b and 9d).

On average, we observed that runoff volume reduction, i.e., the impact of impervious surfaces, is greater for the Rebosola catchment than for the Sadocca catchment. The reason for this can be ascribed to the distance of impervious areas from the catchment outlet: runoff from impervious areas of the Sadocca catchment (i.e., Porto Viro town in Figure 7) has the opportunity of diffusing and infiltrating before reaching the pumping station, whereas runoff from impervious areas of the Rebosola catchment (i.e., Pegolotte town in Figure 3) quickly reaches the outlet.

4. Conclusions

In this paper, a two-dimensional shallow water model, able to also describe the rill flow by a subgrid model of ground topography, is coupled with a conceptualized two-dimensional model for the saturated flow in the topsoil layer which includes infiltration and downward vertical percolation. The equations of both models are suitably averaged over a representative elementary area to yield a subgrid model for the coupled surface-subsurface flow.

In the model, runoff production is mainly controlled by the subsurface model through four parameters: the topsoil layer depth D, the effective porosity n_e, the downward vertical percolation rate f, and the horizontal saturated hydraulic conductivity K. These parameters do have some level of conceptualization, but they still maintain their original physical significance, simplifying the calibration process.

The main advantages of the proposed integrated model are (i) contrary to the uncoupled approach, the model does not require the identification of the proper number, shape, and size of subcatchments that drain to the draining channel network, which is a difficult task in lowland catchments characterized by a nearly flat ground surface; (ii) total rainfall rates can be directly applied as boundary condition; (iii) contrary to the uncoupled approach, the model intrinsically allows to predict the flooding of low-lying or concave areas which are not (or inefficiently) drained; (iv) the model has a relatively small number of parameters, reducing the risk of overparameterization; (v) the model equations are not inherently related to a specific numerical method so that their solution can be achieved through different numerical techniques.

A further advantage stems from the numerical solution of overland flow when water depth is very small. With the coupled model, the storativity coefficient ϑ in the mass balance equation (6) cannot go below n_e, whereas, in the uncoupled, shallow water model $\vartheta = \eta$, and η can become negligibly small at very small water depth [*Defina*, 2000]. Accordingly, the impact of the nonlinearity affecting the mass balance equation (note that ϑ is a h-dependent parameter) is reduced with the coupled model and both numerical stability and mass balance accuracy is increased.

The two test cases show that the model is able to accurately predict the hydrological response to heavy rainfall events in flat or gently sloping lowland catchments. The model also accurately predicts the flooded areas including those which are inefficiently drained. A much wider investigation is required to assess the model performance; however, these preliminary results are encouraging.

Future developments should focus effort on refining the subsurface model, which is largely conceptualized at present. However, improvements must contend with the problem of the overparameterization and should use a comprehensive set of accurate field data.

Acknowledgments
Giuseppe Gasparetto Stori of the "Adige-Euganeo" Land Reclamation Consortium and Giancarlo Mantovani of the "Delta del Po" Land Reclamation Consortium are kindly acknowledged. This research was partially funded by the Provincia di Venezia-Servizio Protezione Civile and by the University of Padova: grants Ass2012_ICEA_01 and Ass2013_ICEA_08. Dingzhi Peng, Simon Mudd, two anonymous reviewers, the first anonymous Associate Editor, and Luis Samaniego (second Associate Editor) are gratefully acknowledged for their comments, which have significantly improved the manuscript.

References

Arnold, J. G., and N. Fohrer (2005), SWAT2000: Current capabilities and research opportunities in applied watershed modelling, *Hydrol. Processes*, *19*, 563–572.
Bates, P. D., and A. P. J. De Roo (2000), A simple raster-based model for flood inundation simulation, *J. Hydrol.*, *236*, 54–77.
Benettin, P., Y. van der Velde, S. E. A. T. M. van der Zee, A. Rinaldo, and G. Botter (2013), Chloride circulation in a lowland catchment and the formulation of transport by travel time distributions, *Water Resour. Res.*, *49*, 4619–4632, doi:10.1002/wrcr.20309.
Beven, K. (1989), Changing ideas in hydrology: The case of physically based model, *J. Hydrol.*, *105*, 157–172.
Beven, K. (2012), *Rainfall-Runoff Modelling: The Primer*, John Wiley, Chichester, U. K.
Borah, D. K. (2011), Hydrologic procedures of storm event watershed models: A comprehensive review and comparison, *Hydrol. Processes*, *25*, 3472–3489, doi:10.1002/hyp.8075.
Botter, G., E. Bertuzzo, and A. Rinaldo (2010), Transport in the hydrologic response: Travel time distributions, soil moisture dynamics, and the old water paradox, *Water Resour. Res.*, *46*, W03514, doi:10.1029/2009WR008371.
Burt, T. P., and M. C. Slattery (1996), Time-dependent changes in soil properties and runoff generation, in *Advances in Hillslope Processes*, edited by M. G. Anderson and S. M. Brooks, pp. 79–95, John Wiley, Chichester, U. K.
Camporese, M., C. Paniconi, M. Putti, and S. Orlandini (2010), Surface-subsurface flow modeling with path-based runoff routing, boundary condition-based coupling, and assimilation of multisource observation data, *Water Resour. Res.*, *46*, W02512, doi:10.1029/2008WR007536.
Carluer, N., and G. De Marsily (2004), Assessment and modelling of the influence of man-made networks on the hydrology of a small watershed: Implications for fast flow components, water quality and landscape management, *J. Hydrol.*, *285*, 76–95.
Cazorzi, F., G. Dalla Fontana, A. De Luca, G. Sofia, and P. Tarolli (2013), Drainage network detection and assessment of network storage capacity in agrarian landscape, *Hydrol. Processes*, *27*, 541–553, doi:10.1002/hyp.9224.
D'Alpaos, L., and A. Defina (2007), Mathematical modeling of tidal hydrodynamics in shallow lagoons: A review of open issues and applications to the Venice lagoon, *Comput. Geosci.*, *33*, 476–496.
Defina, A. (2000), Two dimensional shallow flow equations for partially dry areas, *Water Resour. Res.*, *36*(11), 3251–3264.
Defina, A. (2003), Numerical experiments on bar growth, *Water Resour. Res.*, *39*(4), 1092, doi:10.1029/2002WR001455.
Defina, A., and B. Matticchio (1994), A coupled 2D model for interacting surface water and groundwater flows, in *2nd International Conference on River Flood Hydraulics*, edited by W. R. White and J. Watts, pp. 145–154, John Wiley, Chichester, U. K.
De Roo, A., et al. (2003), Development of a European flood forecasting system, *Int. J. River Basin Manage.*, *1*(1), 49–59.
Duke, G. D., S. W. Kienzle, D. L. Johnson, and J. M. Byrne (2006), Incorporating ancillary data to refine anthropogenically modified overland flow paths, *Hydrol. Processes*, *20*, 1827–1843, doi:10.1002/hyp.5964.
Eck, B. J., M. E. Barrett, and R. J. Charbeneau (2012), Coupled surface-subsurface model for simulating drainage from permeable friction course highways, *J. Hydraul. Eng.*, *138*(1), 13–22.
Fiener, P., K. Auerswald, and K. Van Oost (2011), Spatio-temporal patterns in land use and management affecting surface runoff response of agricultural catchments—A review, *Earth Sci. Rev.*, *106*, 92–104.
Furman, A. (2008), Modeling coupled surface-subsurface flow processes: A review, *Vadose Zone J.*, *7*(2), 741–756, doi:10.1016/j.earscirev.2011.01.004.
Gascuel-Odoux, C., P. Aurousseau, T. Doray, H. Squividant, F. Macary, D. Uny, and C. Grimaldi (2011), Incorporating landscape features to obtain an object-oriented landscape drainage network representing the connectivity of surface flow pathways over rural catchments, *Hydrol. Processes*, *25*, 3625–3636, doi:10.1002/hyp.8089.
Getirana, A. C. V., M. P. Bonnet, O. C. Rotunno Filho, and W. J. Mansur (2009), Improving hydrological information acquisition from DEM processing in floodplains, *Hydrol. Processes*, *23*, 502–514, doi:10.1002/hyp.7167.
Giraldo, F. X. (2000), The Lagrange-Galerkin method for the two-dimensional shallow water equations on adaptive grids, *Int. J. Numer. Methods Fluids*, *33*, 789–832.
Graham, D. N., and M. B. Butts (2005), Flexible, integrated watershed modelling with MIKE SHE, in *Watershed Models*, edited by V. P. Singh and D. K. Frevert, pp. 245–272, CRC Press, Boca Raton, Fla.
Grimaldi, S., A. Petroselli, E. Arcangeletti, and F. Nardi (2013), Flood mapping in ungauged basins using fully continuous hydrologic-hydraulic modeling, *J. Hydrol.*, *487*, 39–47, doi:10.1016/j.jhydrol.2013.02.023.
Hallema, D. W., P. Andrieux, R. Moussa, and M. Voltz (2013), Parameterization and multi-criteria calibration of a distributed storm flow model applied to a Mediterranean agricultural catchment, *Hydrol. Processes*, *27*, 1379–1398, doi:10.1002/hyp.9268.
He, Z., W. Wu, and S. S. Y. Wang (2008), Coupled finite-volume model for 2D surface and 3D subsurface flows, *J. Hydraul. Eng.*, *13*(9), 835–845.
Hunter, N. M., P. D. Bates, M. S. Horritt, and M. D. Wilson (2007), Simple spatially-distributed models for predicting flood inundation: A review, *Geomorphology*, *90*, 208–225.
Ivanov, V. Y., E. R. Vivoni, R. L. Bras, and D. Entekhabi (2004), Catchment hydrologic response with a fully distributed triangulated irregular network model, *Water Resour. Res.*, *40*, W11102, doi:10.1029/2004WR003218.
Kim, J., A. Warnock, V. Y. Ivanov, and N. D. Katopodes (2012), Coupled modeling of hydrologic and hydrodynamic processes including overland and channel flow, *Adv. Water Resour.*, *37*, 104–126, doi:10.1016/j.advwatres.2011.11.009.
Kong, J., X. Pei, Z. Song, and L. Li (2010), A new model for coupling surface and subsurface water flows: With an application to a lagoon, *J. Hydrol.*, *390*, 116–120.
Kumar, R., L. Samaniego, and S. Attinger (2013), Implications of distributed hydrologic model parameterization on water fluxes at multiple scales and locations, *Water Resour. Res.*, *49*, 360–379, doi:10.1029/2012WR012195.
Leavesley, G., and L. Stannard (1995), The precipitation-runoff modeling system PRMS, in *Computer Models of Watershed Hydrology*, edited by V. P. Singh, pp. 281–310, Water Resour. Publ., Highlands Ranch, Colo.
Lerat, J., C. Perrin, V. Andréassian, C. Loumagne, and P. Ribstein (2012), Towards robust methods to couple lumped rainfall-runoff models and hydraulic models: A sensitivity analysis on the Illinois River, *J. Hydrol.*, *418–419*, 123–135.
Levavasseur, F., J. S. Bailly, P. Lagacherie, F. Colin, and M. Rabotin (2012), Simulating the effects of spatial configurations of agricultural ditch drainage networks on surface runoff from agricultural catchments, *Hydrol. Processes*, *26*, 3393–3404, doi:10.1002/hyp.8422.
Li, Q., A. J. A. Unger, E. A. Sudicky, D. Kassenaar, E. J. Wexler, and S. Shikaze (2008), Simulating the multi-seasonal response of a large-scale watershed with a 3D physically-based hydrologic model, *J. Hydrol.*, *357*, 317–336.
Liang, D., R. A. Falconer, and B. Lin (2007), Coupling surface and subsurface flows in a depth averaged flood wave model, *J. Hydrol.*, *337*, 147–158.

Loague, K., C. S. Heppner, B. A. Ebel, and J. E. VanderKwaak (2010), The quixotic search for a comprehensive understanding of hydrologic response at the surface: Horton, Dunne, *Dunton*, and the role of concept-development simulation, *Hydrol. Processes*, *24*, 2499–2505.

Martini, P., L. Carniello, and C. Avanzi (2004), Two dimensional modelling of flood flows and suspended sediment transport: The case of Brenta River, Veneto (Italy), *Nat. Hazards Earth Syst. Sci.*, *4*(1), 165–181.

McMillan, H. K., and J. Brasington (2008), End-to-end flood risk assessment: A coupled model cascade with uncertainty estimation, *Water Resour. Res.*, *44*, W03419, doi:10.1029/2007WR005995.

Morita, M., and B. C. Yen (2002), Modelling of conjunctive two-dimensional surface–three-dimensional subsurface flows, *J. Hydraul. Eng.*, *128*, 184–200.

Moussa, R., M. Voltz, and P. Andrieux (2002), Effects of the spatial organization of agricultural management on the hydrological behaviour of a farmed catchment during flood events, *Hydrol. Processes*, *16*, 393–412, doi:10.1002/hyp.333.

Nester, T., J. Komma, A. Viglione, and G. Blöschl (2012), Flood forecast errors and ensemble spread—A case study, *Water Resour. Res.*, *48*, W10502, doi:10.1029/2011WR011649.

Qu, Y., and C. J. Duffy (2007), A semidiscrete finite volume formulation for multiprocess watershed simulation, *Water Resour. Res.*, *43*, W08419, doi:10.1029/2006WR005752.

Refsgaard, J. C. (1997), Parametrisation, calibration and validation of distributed hydrological models, *J. Hydrol.*, *198*, 69–97.

Samaniego, L., R. Kumar, and S. Attinger (2010), Multiscale parameter regionalization of a grid-based hydrologic model at the mesoscale, *Water Resour. Res.*, *46*, W05523, doi:10.1029/2008WR007327.

Schwanghart, W., G. Groom, N. J. Kuhn, and G. Heckrath (2013), Flow network derivation from a high resolution DEM in a low relief, agrarian landscape, *Earth Surf. Processes Landforms*, *38*, 1576–1586, doi:10.1002/esp.3452.

Sebben, M. L., A. D. Werner, J. E. Liggett, D. Partington, and C. T. Simmons (2012), On the testing of fully integrated surface-subsurface hydrological models, *Hydrol. Processes*, *27*, 1276–1285, doi:10.1002/hyp.9630.

Shen, C., and M. S. Phanikumar (2010), A process-based, distributed hydrologic model based on a large-scale method for surface-subsurface coupling, *Adv. Water Resour.*, *33*, 1524–1541.

Slattery, M. C., P. A. Gares, and J. D. Phillips (2006), Multiple modes of storm runoff generation in a North Carolina coastal plain watershed, *Hydrol. Processes*, *20*, 2953–2969.

Therrien, R., R. G. McLaren, E. A. Sudicky, and S. M. Panday (2005), *HydroGeoSphere: A Three-Dimensional Numerical Model Describing Fully-Integrated Subsurface and Surface Flow and Solute Transport*, 322 pp., Groundwater Simul. Group, Univ. of Waterloo, Waterloo, Ont., Canada.

VanderKwaak, J. E., and K. Loague (2001), Hydrologic-response simulations for the R-5 catchment with a comprehensive physics-based model, *Water Resour. Res.*, *37*(4), 999–1013.

Viero, D. P., A. D'Alpaos, L. Carniello, and A. Defina (2013), Mathematical modeling of flooding due to river bank failure, *Adv. Water Resour.*, *59*, 82–94, doi:10.1016/j.advwatres.2013.05.011.

Walters, R. A., and V. Casulli (1998), A robust, finite element model for hydrostatic surface water flows, *Commun. Numer. Methods Eng.*, *14*, 931–940, doi:10.1002/(SICI)1099-0887(1998100)14:10<931::AID-CNM199>3.0.CO;2-X.

Yuan, D., B. Lin, and R. A. Falconer (2008), Simulating moving boundary using a linked groundwater and surface water flow model, *J. Hydrol.*, *349*, 524–535.

Zhang, J., M. A. Ross, J. S. Geurink, and H. Gong (2010), Modelling vadose zone moisture dynamics in shallow water table settings with the integrated hydrologic model: Field-scale testing and application, *Water Environ. J.*, *24*, 9–20, doi:10.1111/j.1747-6593.2009.00166.x.